Journal of Electrostatics 107 (2020) 103480

Contents lists available at ScienceDirect

Journal of Electrostatics

journal homepage: http://www.elsevier.com/locate/elstat

On the accuracy of an interdigital electrostatic position sensor

L.E. Helseth

Department of Physics and Technology, Allegaten 55, 5020, Bergen, University of Bergen, Norway

ARTICLE INFO

Keywords:
Interdigital electrode
Electrostatics
Motion detection

ABSTRACT

In this work the induced voltage in an interdigital electrode when swept by a finite, triboelectrically charged dielectric surface is investigated. Finite element modelling fits well with the measured voltage as a function of position. An analytical model for the accuracy with which the position of the object can be determined, in presence of noise, is presented. The fundamental limit with which the position can be determined from electrical output data is also discussed, and could act as a useful guideline when estimating the limits of self-powered position sensor systems.

1. Introduction

Monitoring the position of objects or body parts play an important role in developing sensors accompanying a range of applications, from display technology to patient care. Of particular interest, position registration of moving body parts sensors based on induced electric charge have been used to detect human body motion [1–4] or rotational motion of motors [5]. These devices require external power sources, which under certain conditions may hamper their widespread use, thus paving the way for self-powered devices.

Electrostatic actuators and energy harvesting based on electrostatics have a long history [6–8], and more recent research has demonstrated a number of electrostatic devices for vibration energy harvesting [9–13]. Triboelectric nanogenerators are very promising in the development of self-powered devices, and considerable efforts have been devoted to developing self-powered position sensing technology [14–27], for the simple reason that such technologies could be deployed wherever batteries or other electrical power sources are unwanted.

For detection of linear motion, interdigitated electrodes (IDEs) have been found particularly useful, due to low cost and easy implementation of appropriate dimensions [18,19,27]. While considerable research has been undertaken to demonstrate how self-powered position sensors may function and how to generate as much electrical power as possible from such devices, less efforts have been put into validating the electrical parameters against finite element modelling and to estimate the accuracy with which the position can be found. Here, finite element model results are validated against experimental data for an IDE, and this information is used to estimate the positional uncertainty. Furthermore, the fundamental limit to which the position can be determined is also discussed.

2. Experimental setup

The interdigital electrode was created in about 0.01 mm thick aluminum on a polymer substrate using UV-lithography. A positive-negative film (Scankemi, purchased from Elfa Distrelec, art. nr. 149-57-791) was placed under a printed mask and exposed to UV-light for 5 s, after which a soft cover layer was removed such that only the aluminum layer remained on the substrate. For the 4 pairs of fingers, each electrode finger was 4 mm wide and they had a gap of 4 mm between them. The length of the fingers was much larger (50 mm) than the width. A 10 mm wide and 50 mm wide Polydimethylsiloxane (PDMS) block was created using Sylgaard 184 (Dow Chemical Company). A 10:1 elastomer to curing agent ratio was used, poured into a mold and cured overnight at room temperature to obtain the solid block used in the experiments. The dimensions of the IDE and PDMS block were selected to be close to those of human fingers and because the selected dimensions made it easier to do measurements with the available experimental setup and test the finite element simulations against these. The surface of the PDMS block facing the metal interdigitated electrodes (IDE) was first wiped with methanol to remove all surface charge, dried and subsequently charged triboelectrically by pressing the PDMS surface against a flat piece of aluminum. After removing the PDMS from the aluminum, the surface charge on the PDMS was determined from three independent measurements to be $\sigma = -0.21 \pm 0.05\ \mu C/m^2$ using a Desco EMIT 50597 static field meter. PDMS is a good isolator, and the surface charge remained for a duration much longer than each experiment. The PDMS block was mounted on a translation stand, while the IDE was

E-mail address: lars.helseth@ift.uib.no.

https://doi.org/10.1016/j.elstat.2020.103480
Received 29 February 2020; Received in revised form 20 May 2020; Accepted 21 May 2020
Available online 30 May 2020

positioned on a fixed stand, which when needed could be screened by a Faraday cage to avoid buildup of charges from external sources. The PDMS was kept at a fixed height, such that its lower surface was 1 mm above the IDE. The potential difference between the electrodes of the IDE was measured using a Keithley 6514 instrument with input impedance exceeding 10^{14} Ω. Part of the setup is shown in Fig. 1. Each measurement of voltage was repeated three times, and the average value and uncertainty were reported in Fig. 2 b).

3. Potential difference

The potential difference between the interdigital electrodes was simulated using finite element modelling in COMSOL 5.4 (AC/DC module). During modelling, one electrode in the IDE was grounded while the other was floating, as seen in Fig. 1 a). The geometry of the simulation was the same as in the experimental setup. Only PDMS was assigned a surface charge. The surface charge on surface of the PDMS facing the IDE was selected to be $\sigma = -0.21$ μC/m^2, as found experimentally. The potential was found numerically solving the Laplace equation ($\nabla^2\phi = 0$, where ϕ is the potential) with the boundary conditions states above. In order to ensure convergence of the obtained potentials, the mesh was made gradually finer until the variations in the potential between simulations was smaller than a certain value, here set to be 0.1 V. The PDMS slab was translated in steps of 1 mm. For each step, the simulation gave a spatial electric potential distribution, resulting in 20 simulations similar to those in Fig. 2 a). In Fig. 2 a), the leftmost simulation shows the potential distribution where the PDMS surface was directly above a grounded electrode (x = 0 mm), whereas the rightmost simulation shows the situation where the PDMS surface was above a free-floating electrode (x = 8 mm).

The two distinct finite element simulations in Fig. 2 a) are only two of in total 20 simulations undertaken in this study. From each simulation, a figure similar to those shown in Fig. 2 a) was obtained, which allowed extraction of the potential difference between the two interdigital electrodes. The black boxes in Fig. 2 b) show the measured potential difference between the electrodes upon moving the PDMS in steps of 1 mm, while the green boxes show the results of the finite element simulations. It is seen that good agreement is obtained between

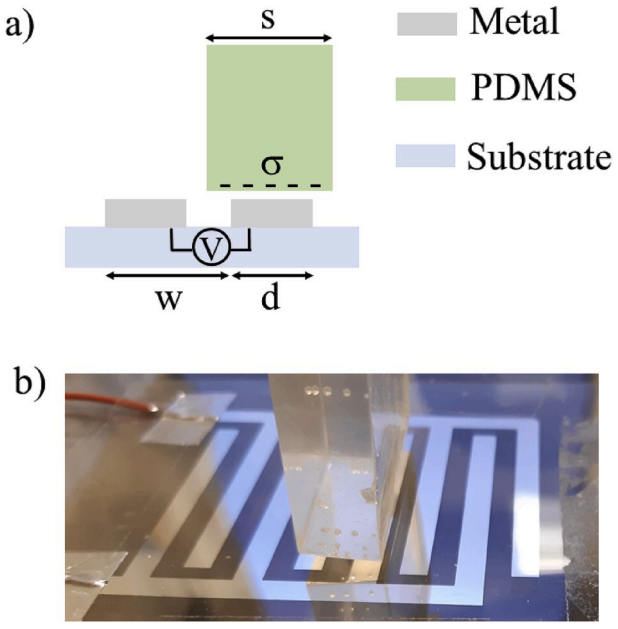

Fig. 1. Schematic drawing of the experimental setup and the dimensions involved (a). The potential difference across the interdigitated electrodes is measured with the instrument labeled 'V'. Here s = 10 mm, w = 8 mm and d = 4 mm. Also shown is a picture of the PDMS slab and the IDE used (b).

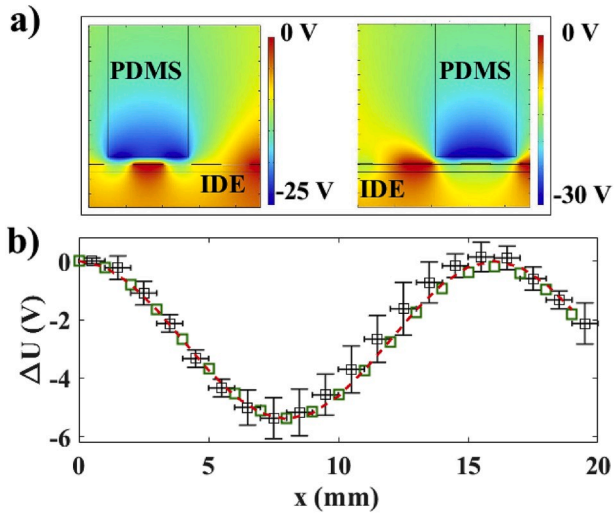

Fig. 2. Figure a) shows finite element simulations of the electrical potential when a PDMS surface of charge −0.21 μC/m^2 is placed directly above an earthed electrode (left) and directly above a floating + electrode (right). In b) the experimental data for the voltage over the interdigitated electrodes as a function of position are shown as black boxes, whereas the finite element simulations are shown as green boxes. A simple analytical function is shown as a red, dashed line. The voltages at x = 0 mm and x = 8 mm were taken from the left and right simulations in a). (For interpretation of the references to colour in this figure legend, the reader is referred to the Web version of this article.)

experimental data and simulations, with no free parameters in the simulations. There is a shift between the measured average values and the numerical simulations in the region between 9 mm and 15 mm. However, since there is overlap between all the numerical finite element simulations and the experimental data after accounting for the uncertainty in the experimental data, there is no conclusive evidence for a shift.

4. Voltage-dependent position noise

The red dashed line in Fig. 2 b) represents the function $\Delta U(x) = U_0\cos(2\pi x/L)-U_0$, with $U_0 = 2.7$ V and L = 16 mm. It is found that such a simple periodic function represents the finite element and the experimental data very well to within experimental uncertainty, and it is therefore suitable for analyzing the smallest position accuracy of the sensor. The smallest change in voltage with position x is found in the region near x = 0 (or subsequent periodical shifts), where $\Delta U(x) \approx -(U_0/2)(2\pi/L)^2x^2$.

Fig. 3 shows two examples of histograms of the number of counts sampled for a particular voltage ΔU for the minimum noisy case when a person is far away and there is shielding (Fig. 3 a) or for a typical situation when the shielding is removed and a person at rest is in the vicinity (Fig. 3 b). None of these experimental distributions are gaussian, and there might be systematic deviations particularly in the case of Fig. 3 b) as suggested by the small deviation from zero. However, using a gaussian to model the probability distributions is perhaps the simplest approach if estimates are to be obtained while keeping essence. The dashed line in Fig. 3 a) is a gaussian probability distribution with standard deviation $U_n = 0.03$ V, whereas the dashed line in Fig. 3 b) corresponds to standard deviation $U_n = 0.5$ V.

If one assumes that the voltage noise measured is random with standard deviation U_n, it can be represented by a normalized probability distribution function P(ΔU) given by

$$P(\Delta U) = \frac{1}{\sqrt{2\pi}U_n} e^{-\frac{\Delta U^2}{2U_n^2}} \quad (1)$$

The voltage noise influences the position with which one is able to

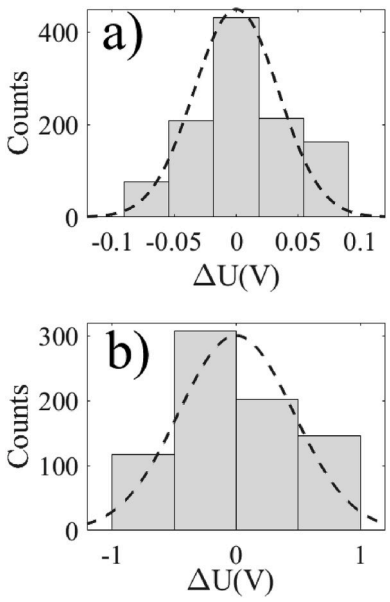

Fig. 3. Histograms of the deviation in voltage from the equilibrium value under different circumstances.

locate the object under study, since voltage is normally translated into position using some algorithm. During readout, a small uncertainty in voltage is translated into a small uncertainty in position dx with probability distribution function given by $P(x) = P(\Delta U)|d\Delta U/dx|$, or

$$P(x) = \frac{4\pi^2 U_0}{L^2\sqrt{2\pi}U_n}|x|e^{-\frac{U_0^2\left(\frac{2\pi^2}{L^2}\right)^2 x^4}{2U_n^2}}. \quad (2)$$

The variance is given by

$$x^2 = \int_{-\infty}^{\infty} x^2 P(x)dx \approx \frac{L^2 U_n}{\pi^2\sqrt{2\pi}U_0}, \quad (3)$$

and by taking the square root one arrives at $\sqrt{x^2} = \left(\frac{1}{\pi^2\sqrt{2\pi}}\right)^{1/2} L\sqrt{U_n/U_0} \approx 0.2L\sqrt{U_n/U_0}$. In the experimental data from Fig. 2 b) one has $U_0 = 2.7$ V, $U_n \approx 0.5$ V and L = 16 mm, thus giving $\sqrt{x^2} \approx 1.4$ *mm*. Here the value $U_n \approx 0.5$ V was used, since the situation without screening represents the worst-case scenario and might be of most interest in self-powered electrostatic sensors. The experimental measurements of position are measured to within an error of ±0.5 mm, which differs from the 1.4 mm estimated assuming gaussian noise voltage fluctuations. It should also be pointed out that the relative position uncertainty $\sqrt{x^2}/L$ is determined by the ratio of noise voltage to signal voltage, and is therefore independent of system size.

The lowest possible measurable noise at a temperature T is the thermal noise given by $U_n^2 \approx k_B T/C$, where k_B is Boltzmann's constant, T is the temperature and C is the capacitance of the electrode. A measure for the smallest uncertainty in position is then

$$\sqrt{x^2} \approx 0.2L\left(\frac{k_B T}{CU_0^2}\right)^{\frac{1}{4}}. \quad (4)$$

It is therefore seen that the fractional observed fluctuations in the position, $\beta = \sqrt{x^2}/L$, is determined by the ratio of the thermal energy of one degree of freedom ($1/2k_BT$) to the stored energy of the capacitor ($1/2CU_0^2$). In the experimental system reported in this manuscript C ≈ 5 pF and T = 296 K, which gives $U_n \approx 29$ μV. If $U_0 = 2.7$ V, and L = 16 mm one obtains an estimate of the smallest resolvable uncertainty to be $\sqrt{x^2} \approx 0.01$ *mm*. This is far beyond the capability of the experimental system studied here, mainly due to the difficulties found screening all external influences even in presence of a suitable Faraday cage. However, the limit in Eq. (4) could be a useful guideline when estimating the limits of a self-powered position sensor system.

5. Conclusion

In this study finite element simulations of an electrostatic position sensor are validated against experimental data, with no free parameters. This information is used to estimate the positional uncertainty, and the fundamental limits to which the position can be determined is discussed. While interdigital electrodes for position detection have been used as an example here, it is straightforward to apply the analysis presented to other self-powered position sensor systems. As such, the approach presented here might contribute to the understanding of the limits of self-powered electrostatic position sensors.

Declaration of competing interest

The authors declare that they have no known competing financial interests or personal relationships that could have appeared to influence the work reported in this paper.

References

[1] K. Kurita, Y. Fujii, K. Shimada, A new technique for touch sensing based on measurement of current generated by electrostatic induction, Sensor. Actuator. A 170 (2011) 66–71.
[2] K. Kurita, Novel non-contact and non-attached technique for detecting sports motion, Measurement 44 (2011) 1361–1366.
[3] W. Zheng, Z.Z. Cui, Z. Zheng, Y. Zhang, Remote monitoring of human hand motion using induced electrostatic signals, J. Electrost. 69 (2011) 571–577.
[4] X. Chen, Z. Zheng, Z.Z. Cui, W. Zheng, A novel remote sensing technique for recognizing human gait based on the measurements of induced electrostatic current, J. Electrost. 70 (2012) 105–110.
[5] L. Wang, Y. Yan, Mathematical modelling and experimental validation of electrostatic sensors for rotational speed measurement, Meas. Sci. Technol. 25 (2014) 115101.
[6] O. Jefimenko, D.K. Walker, Electrostatic motors, Phys. Teach. 9 (1971) 121.
[7] O. Jefimenko, Operation of electric motors from the atmospheric electric field, Am. J. Phys. 39 (1971) 776.
[8] O. Jefimenko, D.K. Walker, Electrostatic current generator having a disk electret as an active element, IEEE Trans. Ind. Appl. IA-14 (1978) 537–540.
[9] P.D. Mitcheson, T. Sterken, C. He, M. Kiziroglou, E.M. Yeatman, R. Puers, "Electrostatic microgenerators", Measurement and Control 41 (2008) 114–119.
[10] Y. Sakane, Y. Suzuki, N. Kasagi, The development of a high-performance perfluorinated polymer electret and its application to micro power generation, J. Micromech. Microeng. 18 (2008) 104011.
[11] Y. Suzuki, Recent progress in MEMS electret generator for energy harvesting, IEEJ Trans. Electr. Electron. Eng. 6 (2011) 101–111.
[12] F.U. Khan, M.U. Quadir, State-of-the-art in vibration-based electrostatic energy harvesting, J. Micromech. Microeng. 26 (2016) 103001.
[13] J. Hillenbrand, P. Pondrom, G.M. Sessler, Electret transducer for vibration-based energy harvesting, Appl. Phys. Lett. 106 (2015) 183902.
[14] Y. Su, G. Zhu, W. Yang, J. Yang, J. Chen, Q. Jing, Z. Wu, Y. Jiang, Z.L. Wang, Triboelectric sensor for self-powered tracking of object motion inside tubing, ACS Nano 8 (2014) 3843–3850.
[15] Q. Jing, Y. Xie, G. Zhu, R.P. Shan, Z.L. Wang, Self-powered thin-film motion vector sensor, Nat. Commun. 6 (2015) 8031.
[16] Q. Jing, Y.S. Choi, M. Smith, N. Catic, C. Ou, S. Kar-Narayan, Aerosol-jet printed fine-featured triboelectric sensors for motion sensing, Adv. Mater. Technol. 4 (2019) 1800328.
[17] L. Dhakar, P. Pitchappa, F.E.H. Tay, C.K. Lee, An intelligent skin based self-powered finger motion sensor integrated with triboelectric nanogenerator, Nano Energy 19 (2016) 532–540.
[18] B. Meng, W. Tang, Z.H. Too, X. Zhang, M. Han, W. Liu, H.X. Zhang, A transparent single-friction-surface triboelectric generator and self-powered touch sensor, Energy Environ. Sci. 6 (2016) 3235–3240.
[19] H. Wu, Z. Su, M. Shi, L. Miao, Y. Song, H. Chen, M. Han, H.X. Zhang, Self-powered noncontact electronic skin for motion sensing, Adv. Funct. Mater. 28 (2017) 170464.
[20] L.E. Helseth, Interdigitated electrodes based on liquid metal encapsulated in elastomer as capacitive sensors and triboelectric nanogenerators, Nano Energy 50 (2018) 266–272.
[21] H. Guo, X. Jia, L. Liu, X. Cao, N. Wang, Z.L. Wang, Freestanding triboelectric nanogenerator enables noncontact motion-tracking and positions, ACS Nano 12 (4) (2018) 3461–3467.

[22] L.E. Helseth, Triboelectric proximity and contact detection using soft planar spiral electrodes, Smart Mater. Struct. 28 (2019), 095009.
[23] Y. Xi, J. Hua, Y. Shi, Noncontact triboelectric nanogenerator for human motion monitoring and energy harvesting, Nano Energy 69 (2020) 104390.
[24] Y. Tang, H. Zhou, X. Sun, N. Diao, J. Wang, B. Zhang, C. Qin, E. Liang, Y. Mao, Triboelectric touch-free screen sensor for noncontact gesture recognizing, Adv. Funct. Mater. 30 (2020) 1907893.
[25] R. Zhang, M. Hummelgård, J. Örtegren, M. Olsen, H. Andersson, Y. Yang, H. Olin, Human body constituted triboelectric nanogenerators as energy harvesters, code transmitters, and motion sensors, ACS Appl. Energy Mater. 61 (2018) 2955–2960.
[26] R. Zhang, M. Hummelgård, J. Örtegren, Y. Yang, H. Andersson, E. Balliu, N. Blomquist, M. Engholm, M. Olsen, Z.L. Wang, H. Olin, Sensing body motions based on charges generated on the body, Nano Energy 63 (2019) 103842.
[27] J. Zhu, X. Guo, D. Meng, M. Cho, I. Park, R. Huang, W. Song, A flexible comb electrode triboelectric-electret nanogenerator with separated microfibers for a self-powered position, motion direction and acceleration tracking sensor, J. Mater. Chem. 6 (2018) 16548.